cosmetics

MDPI

Article

Early Detection of Lamellar Gel Network Instability in Cosmetic Emulsions Using Rheology, Laser Diffraction, and AI-Assisted Microscopy

Axel Viton [1,2,*], Raphaël Coatmeur [2], Béatrice Anthouard [1], Magalie Claeys-Bruno [2], Christophe Sauzet [2] and Philippe Piccerelle [2]

[1] Laboratoire SICAF Cosmétiques, 367 All. Bellecour, 84200 Carpentras, France
[2] CNRS, IRD, IMBE, Avignon Université, Aix-Marseille University, 13385 Marseille, France; raphael.coatmeur@univ-amu.fr (R.C.); m.claeys-bruno@univ-amu.fr (M.C.-B.); christophe.sauzet@univ-amu.fr (C.S.)
* Correspondence: axelviton@hotmail.fr

Abstract

Standard ISO testing of cosmetic emulsions offers limited insight into the microstructural mechanisms governing long-term stability. We hypothesize that a single weight-percent increase in emulsifier concentration is sufficient to determine, through its effect on inter-bilayer junction connectivity, whether the lamellar gel network consolidates or fails. To test this, we apply a two-tier strategy combining ISO/TR 18811 testing and Turbiscan turbidimetry with rheology, laser diffraction, and AI-assisted polarized light microscopy, on two oil-in-water emulsions structured by a lamellar gel network and stabilized by Cetearyl Alcohol/Cetearyl Glucoside at 2 wt% (Emulsion A) and 3 wt% (Emulsion B) over 30 days of storage. First-tier testing distinguished formulations only at Day 30; Turbiscan index values (2.64, 1.78) stayed below threshold throughout. The second-tier protocol resolved structural divergence from Day 8 to 15, two to three weeks earlier. In Emulsion A, a transient birefringent fraction (51.5% at Day 8) preceded network disruption, droplet coalescence, and a drift of the loss tangent toward more liquid-like values. In Emulsion B, birefringence expanded to 98.4% by Day 30 and the loss tangent declined to 0.325. These results indicate that a 1 wt% difference in emulsifier concentration, within a range of industrial use, is sufficient to determine whether the lamellar gel network consolidates or fails, and that combining rheology, laser diffraction and AI-assisted microscopy resolves this divergence two to three weeks before conventional ISO criteria are met.

Keywords: lamellar gel network; cosmetic emulsion stability; cetearyl alcohol/cetearyl glucoside; polarized light microscopy; oscillatory rheology

Check for updates

Academic Editor: Luis Alfonso Trujillo-Cayado

Received: 26 June 2026
Revised: 3 August 2026
Accepted: 7 August 2026
Published: 12 August 2026

Copyright: © 2026 by the authors. Licensee MDPI, Basel, Switzerland. This article is an open access article distributed under the terms and conditions of the Creative Commons Attribution (CC BY) license.

1. Introduction

Cosmetic emulsion stability is routinely assessed using ISO/TR 18811:2018 protocols, which provide standardized pass/fail criteria but are insensitive to the microstructural changes that govern long-term robustness [1,2]. This limitation is particularly consequential for lamellar systems, where formulation stability depends on a supramolecular organization that can deteriorate or mature over weeks without any macroscopic signature detectable by conventional methods [3,4].

Cetearyl Alcohol (CA) and Cetearyl Glucoside (CG) emulsions are a representative example of this class. Upon cooling, CA and CG co-crystallize to form interdigitated

bilayers that swell in the presence of water, building a three-dimensional lamellar gel network that confers emulsion stability [5,6]. The cohesion of this network is critically dependent on surfactant concentration: below a critical concentration, inter-bilayer junction density is insufficient to maintain network continuity and the system remains prone to destabilization; above it, a topologically continuous, elastically dominant gel forms and long-term stability is achieved [7–10]. Conventional ISO protocols, designed to detect macroscopic failure, cannot resolve the structural divergence that follows from it. CA/CG systems are also of direct industrial interest, as both components are of natural origin, CA from vegetable fatty alcohols and CG by enzymatic glycosylation of plant-sourced glucose, and are compatible with COSMOS and Ecocert certification frameworks [11–16].

The present study was designed to address this analytical gap. The experimental design reflects a deliberate industrial logic: Turbiscan turbidimetry and ISO/TR 18811 testing constitute the first analytical tier, representing the screening tools already deployed in cosmetic quality control. The second tier, oscillatory rheology, laser diffraction granulometry, and DINO-assisted polarized light microscopy, was selected for its accessibility. Building on a multi-technique protocol previously shown to detect instability in cosmetic emulsions [2], we apply this approach to lamellar CA/CG systems and ask whether a 1 wt% difference in surfactant concentration produces resolvable signatures across rheological, laser diffraction, turbidimetric, and microscopic dimensions before conventional criteria are met.

The primary objectives are twofold: first, to elucidate the structural and mechanical mechanisms governing lamellar network stability as a function of emulsifier concentration, and second, to identify analytically tractable parameters capable of capturing this structural divergence earlier and with greater sensitivity than the ISO/Turbiscan industrial baseline, thereby reducing time-to-decision in formulation development and quality control.

2. Materials and Methods

To test this hypothesis, two oil-in-water emulsions structured by a lamellar gel network, a mixed-emulsifier (fatty alcohol/alkyl polyglucoside) system, were formulated using Cetearyl Alcohol/Cetearyl Glucoside at 2 and 3 wt%, respectively, differing by a single weight percent, and subjected to a systematic multi-technique analytical protocol alongside conventional ISO/TR 18811-2018 assessments over 30 days at 25 °C and storage time, assessed at five time points spanning one month (Days 2, 8, 15, 22, and 30). Three independent replicates were prepared.

2.1. Emulsion Formulation and Processing

The two formulations examined in this work originate from an industrial subcontracting project rather than from an experimental design. The original marketed formula contained 2 wt% Cetearyl Alcohol/Cetearyl Glucoside. Routine stability monitoring according to ISO/TR 18811:2018 identified phase separation after one month of storage, and the formula was subsequently corrected by raising the emulsifier content to 3 wt%, which restored compliance. The remaining composition, including the lipid phase, the active ingredient and the rheology modifiers, was left unchanged, so that the two versions differ solely by a 1 wt% increment in emulsifier. Both concentrations lie within the supplier's recommended use range for this Cetearyl Alcohol/Cetearyl Glucoside blend (1–3 wt% for a lotion; Seppic technical datasheet). For the present study, a dedicated batch of each version was manufactured under identical processing conditions and from identical raw material lots, and both were monitored in parallel by the ISO/TR 18811 protocol and by the second-tier techniques. The ISO results reported in Section 3.1 thus reproduce, on an independent batch, the industrial observation from which the study proceeds.

The industrial oil-in-water emulsions contained a 17.5 wt% lipid phase and an active fraction, together with minor amounts of standard cosmetic excipients (rheology modifiers, a preservative system, fragrance and a pH-adjusting acid), the balance being the aqueous phase carrying the emulsifier. The lipid phase combined liquid emollient esters with a minor solid, crystallizing fraction of hydrogenated vegetable glycerides; it is this solid fraction, together with the fatty alcohol of the emulsifier, that takes part in the crystalline bilayer assembly. The active fraction consisted of hyaluronic acid and glycolic acid. As these are commercial formulations produced under industrial subcontract, their full qualitative and quantitative INCI composition is subject to confidentiality and is not disclosed in detail; only the constituents relevant to the present analysis are specified. The lipid phase, the active fraction and the acid content were identical in both formulations, which differ solely by a 1 wt% increment in Cetearyl Alcohol/Cetearyl Glucoside content. The final pH, adjusted with lactic acid, was 5.17 for Emulsion A and 5.07 for Emulsion B. Both formulations used identical raw-material batches and manufacturing conditions, isolating the effect of emulsifier concentration.

The influence of these acids on the lamellar assembly also deserves comment. These pH values lie above the range in which the glycosidic bond of alkyl polyglucosides undergoes appreciable acid-catalysed hydrolysis, and the ISO monitoring recorded compliant pH values at every time point in both formulations [11]. The acid content and the resulting pH were furthermore matched between the two emulsions, and the slightly lower value was measured in Emulsion B, which proved stable, so that acidity cannot account for the divergence reported here.

At the 25 °C storage temperature, the alkyl chains of the Cetearyl Alcohol/Cetearyl Glucoside assembly lie below their melting transition, so that the structure corresponds to a lamellar gel phase rather than to a lamellar liquid-crystalline phase, in which the chains would be molten [6,17]. The assignment to a lamellar gel network rests on the birefringence observed under crossed polarizers (Section 2.4.2), on the crystalline state of the alkyl chains at the storage temperature, and on the phase behaviour documented for fatty alcohol and alkyl polyglucoside systems [4–6,14,17,18]. Small-angle X-ray scattering, which would establish the lamellar repeat distance directly, was not performed, and the geometry of the phase is therefore inferred from these converging observations rather than measured.

Preparation protocol: Aqueous and oil phases were weighed and prepared separately and heated at 75 °C. The oil phase was incorporated slowly into the aqueous phase under vigorous mechanical stirring (900 rpm), followed by 10 min of high-speed homogenization for optimal droplet dispersion and lamellar network development. pH was measured and adjusted using lactic acid. Finished emulsions were packaged, labeled, and submitted to stability protocols.

2.2. Protocol ISO/TR 18811:2018

In the cosmetics industry, monitoring the stability of emulsions involves regular measurements conducted under a range of environmental conditions, including room temperature, 40 °C, 50 °C, 4 °C, under natural light, and in complete darkness. These tests are performed at predefined time intervals to evaluate a set of key parameters, including organoleptic properties (appearance, color, odor, and texture), Brookfield viscosity, pH, and behavior under centrifugation. This extensive monitoring allows for the early detection of physical and chemical instabilities such as phase separation, sedimentation, or degradation of sensitive ingredients.

2.3. Turbidimetry

We used a Turbiscan Lab expert from MICROTRAC (3-5 Rue Paule Raymondis, 31200 Toulouse). It operates based on multi-angle light scattering in transmission (at 880 nm) and backscattering modes, enabling the detection of destabilization phenomena such as sedimentation, flocculation, coalescence or particle migration with high spatial and temporal resolution. The emulsion was taken d + 4 after formulation. The cell was placed for 7 days at 50 °C with a scan every hour. The total number of scans was 161. The TSI was then studied [19].

$$\mathrm{TSI} = \sum(\mathrm{i}=1)^{\mathrm{N}} \sum(\mathrm{j}=1)^{\mathrm{M}} \left|\mathrm{S_{I,j}}(\mathrm{t}+\Delta\mathrm{t}) - \mathrm{S_{I,j}}(\mathrm{t})\right|$$

where $S_{I,j}(t)$ is the transmission or backscattering signal at time t; i represents the position in height within the sample (scan); j represents the type of signal (transmission or backscattering); Δt is the time interval between two successive measurements; N is the number of positions analysed in the sample; and M is the number of signal types considered.

2.4. Microscopy

2.4.1. Bright-Field Optical Microscopy

Droplet morphology was monitored by bright-field light microscopy under transmitted light illumination. Samples were prepared as thin films between glass slides and observed at ×10 magnification (additional magnifications of ×20, ×40, and ×100 were also employed where required). Image acquisition was performed using Leica acquisition software 3.7 in standard mode. Images were recorded at a resolution of 6.3 megapixels (3072 × 2048 pixels, 3:2 aspect ratio) with an exposure time of 250 ms and a gain of 1.00. Transmitted light intensity was adjusted to optimise image quality, with a diaphragm aperture set to 14 and a TL-Fld value of 27. Colorimetric settings were standardised across all acquisitions, with white balance adjusted through the software and fixed channel offsets applied alongside a saturation value of 62.

2.4.2. Polarized Light Microscopy and Image Segmentation

Polarized light microscopy (PLM, Leica DM series 4 Wetzlar, Germany) was employed to visualize the Maltese crosses produced by the optically anisotropic bilayer domains of the lamellar gel network [4,5,15]. The presence, persistence or disappearance of these domains during storage was used as an indicator of the extent of ordered bilayer material within and around droplets.

To quantify the evolution of birefringent domains in an objective and reproducible manner, a patch-based image analysis pipeline was developed. Each micrograph was first normalized by its 99th intensity percentile to account for inter-image illumination variability while preserving the relative intensity of birefringent structures. Patches of 224 × 224 pixels were then extracted with a stride of 112 pixels, giving 50% overlap in both directions. Patches whose mean intensity fell below 15 on the 0 to 255 scale were discarded as background, which excluded 3.9% of patches on average (range 0 to 25% across images) and left 375 patches per micrograph on average (3749 patches over the ten images). Each retained patch was encoded with DINOv2 (ViT-S/14), a Vision Transformer pre-trained by self-supervised learning [20–22], used as a frozen feature extractor without fine-tuning, taking the class token as a 384-dimensional descriptor. Features were standardized to zero mean and unit variance across the whole dataset, so that all time points and both formulations share a common feature space, and partitioned by k-means with k = 2, n_init = 15 and a fixed random seed [23]. The number of clusters was selected by comparing the mean silhouette coefficient for k = 2 to 4, which was maximal at k = 2. Cluster identity was assigned using the Day 2 micrographs, at which both formulations are expected to be

predominantly isotropic, and held fixed for all other time points. Analyses were performed with PyTorch 2.11 and scikit-learn 1.8.

2.5. Rheological Characterization

Rheological measurements were carried out using a TA Instruments Discovery DHR-2 rheometer (TA Instruments, New Castle, DE, USA) equipped with a 40 mm sandblasted parallel-plate geometry. The loading gap was initially set to 1.100 mm and trimmed to 1.000 mm for analysis. All tests were performed at 25 °C, with temperature precisely controlled by a Peltier system. To delineate the linear viscoelastic (LVE) domain, a stress sweep was conducted from 0.01% to 1000% at 0.1 Hz. A frequency sweep was then carried out within the LVE domain at a fixed stress of 0.1%, spanning 0.01–40 Hz to obtain $G'(\omega)$, $G''(\omega)$, and complex viscosity. Data acquisition and analysis were performed using TRIOS software (vesion 6.1).

Measurements were performed at 25 °C. For each condition (emulsion and storage day), three independent repetitions were carried out, giving a total of 30 frequency-sweep tests. The primary rheological variable extracted from each frequency sweep was the loss tangent $\tan\delta = G''/G'$, computed point-wise across the full frequency range and averaged to yield a single representative value per condition. Raw $G'(\omega)$ and $G''(\omega)$ curves were subjected to Savitzky–Golay smoothing prior to $\tan\delta$ computation, in order to reduce high-frequency noise while preserving the overall spectral shape [24]. Temporal evolution of $\tan\delta$ was characterized by plotting condition means with the standard error of the mean (number of repetition $n = 3$) across storage time, and interpreted through descriptive trend analysis.

2.6. Laser Diffraction

Droplet size distributions were measured by laser diffraction using a Mastersizer 3000 (Malvern Instruments, Worcestershire, UK) [25]. The refractive index of the dispersant (water) was set to 1.33, while emulsion refractive indices were determined from fatty phase measurements using an Anton Paar GmbH, Graz, Austria Abbemat 3A0 refractometer (1.4395 and 1.4402 for emulsions A and B, respectively). Measurements were conducted in a hydro dispersion unit at approximately 1300 rpm, adjusted to maintain obscuration between 8% and 20%. Six technical replicates were performed per measurement condition.

Droplet size data were analysed using a linear mixed-effects model (LMM) implemented in Python [26]. The model included emulsion type (A or B), storage time (Days 2, 8, 15, 22, and 30), and their interaction as fixed effects, and replicate group as a random intercept to account for between-replicate variability in baseline Dv50. Statistical significance was assessed at the conventional threshold of $\alpha = 0.05$. All reported p-values correspond to the fixed-effect interaction terms, estimated by the model against the Day 2 baseline of Emulsion A.

3. Results

Results are presented following the two-tier analytical logic described in the Methods. The first-tier assessment, ISO/TR 18811-2018 and Turbiscan turbidimetry, establishes the macroscopic stability baseline using tools representative of standard industrial practice. The second tier, optical and polarized light microscopy, oscillatory rheology, and laser diffraction granulometry, is then applied to resolve the structural divergence between formulations at earlier time points and at greater mechanistic depth.

3.1. First-Tier Assessment: ISO/TR 18811-2018 and Turbiscan Turbidimetry

To establish the macroscopic stability baseline, both formulations were first evaluated against the full ISO/TR 18811-2018 parameter set; the outcomes are summarized in Table 1.

Table 1. Monitoring of the stability of Emulsions A and B according to the ISO monitoring protocol.

Emulsion	Parameter	Day 2	Day 8	Day 15	Day 22	Day 30
Emulsion A	Organoleptic	✓	✓	✓	✓	✗
	pH	✓	✓	✓	✓	✓
	Brookfield viscosity	✓	✓	✓	✓	✓
	Centrifugation	✓	✓	✓	✓	✗
Emulsion B	Organoleptic	✓	✓	✓	✓	✓
	pH	✓	✓	✓	✓	✓
	Brookfield viscosity	✓	✓	✓	✓	✓
	Centrifugation	✓	✓	✓	✓	✓

Monitoring according to ISO/TR 18811-2018 revealed divergent stability profiles between emulsions A and B. Emulsion A failed organoleptic compliance at Day 30 under 50 °C storage, with visible surface oil release indicative of phase separation, and exhibited centrifugation non-compliance at Day 30, while maintaining acceptable pH and Brookfield viscosity throughout. Emulsion B demonstrated full compliance across all ISO parameters over the 30-day assessment period Table 1. While these ISO results confirm the macroscopic divergence between formulations, they provide no information on the underlying microstructural mechanisms.

Turbiscan turbidimetry was evaluated in parallel as the second component of the first-tier industrial baseline. Under accelerated conditions (50 °C, 7 days), both formulations were characterized using the Turbiscan Stability Index (TSI); the resulting backscattering and transmission profiles are shown in Figure 1.

Turbidimetry under accelerated conditions (50 °C) yielded a TSI of 2.64 for Emulsion A and 1.78 for Emulsion B. Both values fall below the conventional stability threshold (TSI < 3). As a single measurement was performed per formulation, the difference of 0.86 units cannot be interpreted quantitatively, and turbidimetry did not provide a basis for discriminating the two formulations under these conditions.

The first-tier results establish the macroscopic ground truth: Emulsion A is unstable and Emulsion B is stable over 30 days of storage. However, neither the ISO/TR 18811-2018 criteria nor the Turbiscan TSI provide any indication of when, how, or at what structural level the divergence originates. This motivates the systematic application of the second-tier protocol, which is designed specifically to address these mechanistic questions.

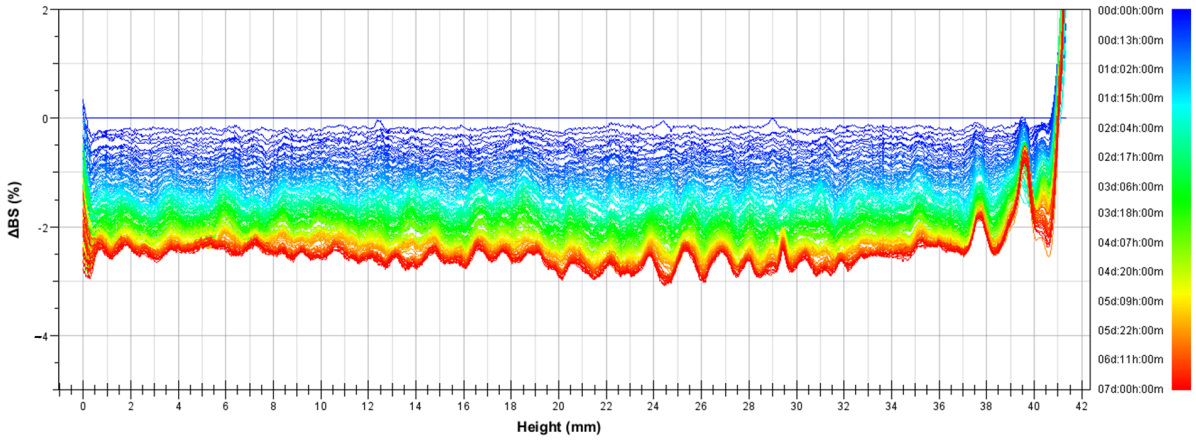

Figure 1. *Cont.*

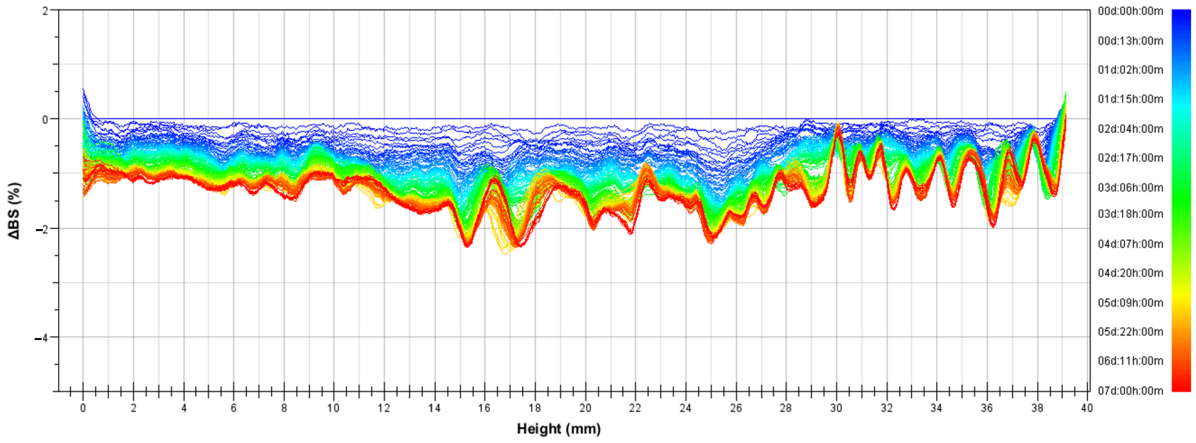

Figure 1. Turbidimetry backscattering (BS) and transmission (T) profiles recorded over 7 days at 50 °C (one scan per hour, 161 scans total) for Emulsion A (TSI = 2.64, left panel) and Emulsion B (TSI = 1.78, right panel), using a Turbiscan Lab Expert (Formulaction, λ = 880 nm). Local signal variations along the cell height reveal mass fluxes associated with migration, flocculation or coalescence events. Both TSI values fall below the conventional threshold (TSI < 3); as a single measurement was acquired per formulation (n = 1), the difference of 0.86 units is not interpreted quantitatively.

3.2. Second-Tier Assessment: Microscopy, Rheology and Laser Diffraction Analysis

Having established that the first-tier methods confirm macroscopic divergence only at Day 30 without resolving its structural origin, the second-tier techniques were applied to probe the emulsions at the droplet and network scale. Optical and polarized light microscopy were used first, providing direct visualization of droplet morphology and lamellar ordering throughout the storage period.

3.2.1. Bright-Field Optical Microscopy

Emulsion A exhibited progressive droplet coalescence from the earliest time points, with small discrete droplets merging into increasingly large structures, consistent with a destabilization of the interfacial films at the 2 wt% emulsifier concentration Figure 2. Coalescence events became clearly discernible from Day 8, with a marked increase in the proportion of large droplets relative to Day 2, and continued to intensify through Day 15 and beyond. By contrast, Emulsion B maintained stable droplet morphology throughout the entire 30-day storage period, with no visible coalescence or phase separation, confirming that the higher emulsifier concentration (3 wt%) conferred sufficient interfacial coverage to sustain both morphological and internal structural integrity.

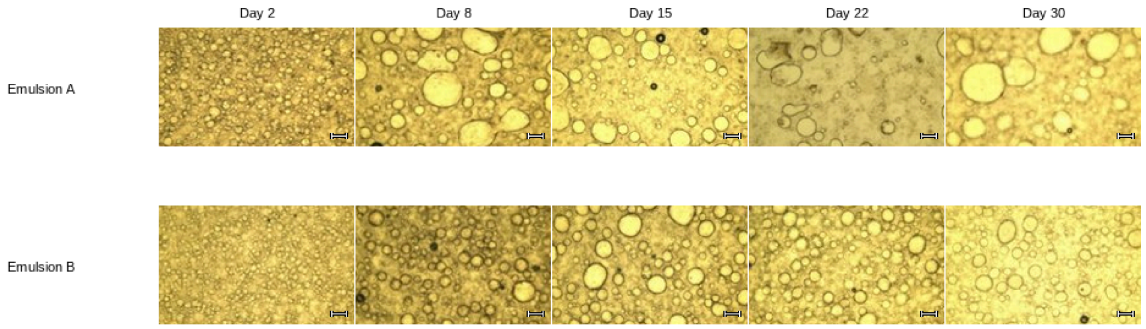

Figure 2. Morphological evolution of Emulsions A and B during isothermal storage at 25 °C, observed by bright-field optical microscopy at Days 2, 8, 15, 22 and 30. Emulsion A (upper row) exhibits progressive coalescence, evidenced by the appearance of increasingly large droplets over time. Emulsion B (lower row) maintains droplet integrity throughout the storage period, with no visible signs of coalescence or phase separation. Scale bar (bottom right of each panel): 100 µm.

Bright-field microscopy thus provides an unambiguous morphological verdict: coalescence in Emulsion A is detectable from Day 8, two to three weeks before ISO criteria are triggered, whereas Emulsion B shows no morphological degradation over the full storage period. These observations prompt a more targeted investigation of the internal lamellar organization using polarized light microscopy.

3.2.2. Polarized Light Microscopy and Segmentation

To complement the morphological information provided by bright-field imaging, polarized light microscopy was used to target the birefringent bilayer domains of the lamellar gel network within and around droplets. A DINO-based patch segmentation pipeline was developed to quantify the evolution of these domains in an objective and reproducible manner Figure 3.

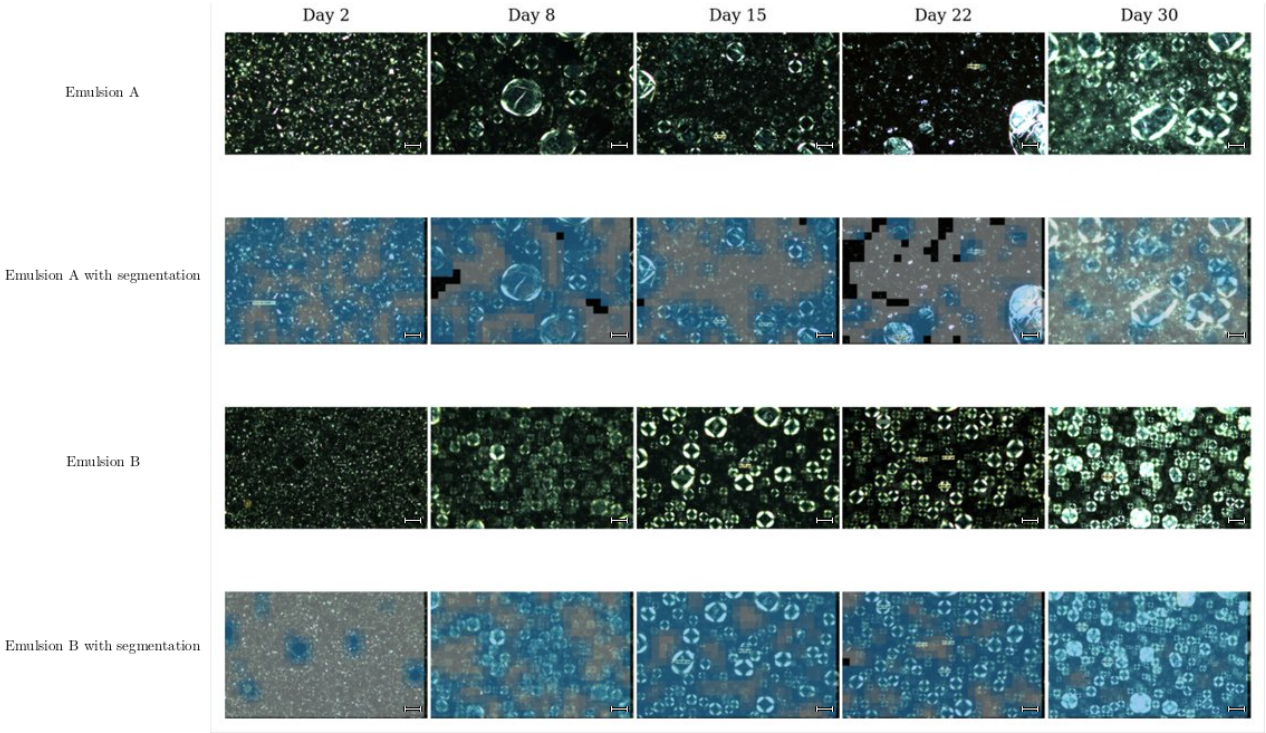

Figure 3. Polarized-light micrographs and DINO segmentation maps of Emulsions A and B during storage at 25 °C (Days 2, 8, 15, 22 and 30). For each emulsion the upper row shows the polarized-light image and the lower row the corresponding segmentation. In Emulsion A the birefringent domains that appear by Day 8 are progressively lost, whereas in Emulsion B the Maltese crosses persist and intensify from Day 8 through Day 30, indicating progressive densification of the internal lamellar gel network. Blue patches (birefringent) correspond to regions displaying optical anisotropy such as Maltese crosses or ordered bilayer domains; gray patches (non-birefringent) indicate isotropic regions with no polarized-light signal; black areas represent the dark background excluded from classification due to insufficient brightness (mean pixel value < 15). Scale bar (bottom right of each panel): 100 µm.

The correspondence between the automatic partition and expert perception was assessed on 250 patches sampled across both formulations and all time points and annotated blind to the clustering output. Excluding 5.6% of patches judged indeterminate, the k-means labels agreed with the expert on 75.0% of cases (Cohen's kappa 0.50; precision 0.73 and recall 0.80 for the birefringent class). Agreement increased with the confidence of the assignment, from 57% for the least to 87% for the most confident patches (kappa 0.74 for the most confident 44%), while the mean silhouette coefficient confirmed that a two-cluster

partition was internally optimal (0.099 at k = 2 versus 0.095 and 0.080 at k = 3 and 4). Two limitations follow. Birefringence is a continuous property, whereas k-means imposes a hard partition, so a partially ordered patch is assigned entirely to one class; the reported fractions therefore describe the proportion of patches whose texture is closer to the ordered than to the isotropic cluster, not the physical fraction of ordered material. In addition, the analysis is performed on two-dimensional sections and cannot represent the three-dimensional organization of the network.

At Day 2, both emulsions appeared predominantly isotropic, with birefringent patch fractions below 11% (10.9% for Emulsion A, 6.8% for Emulsion B), consistent with a disordered, fluid-like internal organization. Beyond Day 8, however, the two formulations diverged markedly. In Emulsion A, the birefringent fraction reached 51.5% at Day 8 but declined progressively to 28.8% at Day 15 and 25.3% at Day 22, reflecting the disruption of the transiently formed anisotropic domains. At Day 30, the corrected birefringent fraction was 26.2% of deformed birefringent structures within coalesced droplets on the basis of their attenuated DINO feature signature. In Emulsion B, the strong birefringence onset at Day 8 (66.7%) was sustained and amplified throughout storage, reaching 87.0%, 86.0% and 98.4% at Days 15, 22 and 30, respectively, reflecting the progressive consolidation of stable internal lipid ordering. The resulting birefringent fraction trajectories are presented in Figure 4.

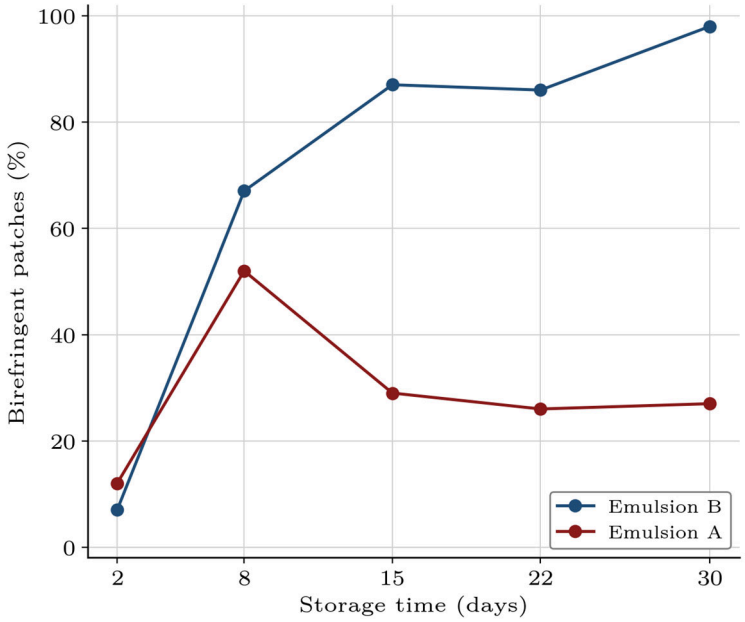

Figure 4. Time evolution of the birefringent patch fraction (%) quantified by DINO patch-level clustering for Emulsion A (unstable, dashed red squares) and Emulsion B (stable, solid blue circles). The value at Day 30 for Emulsion A was corrected to exclude deformed birefringent structures associated with coalesced droplets.

In summary, the DINO-assisted PLM analysis resolves a clear and quantitatively tractable divergence between the two formulations from Day 8 onwards, a full three weeks before ISO criteria are met. The birefringent fraction trajectories—a transient peak followed by decline in Emulsion A, versus a sustained expansion to near-complete ordering in Emulsion B—constitute the earliest and most structurally informative signature of the differential lamellar network fates. Whether this microscopic divergence is also reflected in the bulk mechanical properties of the emulsions is addressed in the next section.

3.3. Rheological Properties

To complement these microstructural observations with macroscopic mechanical data, oscillatory rheology was performed in parallel [27]. Loss tangent (tan δ = G″/G′) was used as the primary rheological indicator to track the balance between viscous and elastic contributions during storage.

The loss tangent (tan δ = G″/G′), tracked over storage as a frequency-sweep average Figure 5, provided a complementary mechanical dimension to the microscopic observations. For Emulsion A, tan δ remained near-constant throughout storage (0.346 ± 0.003), despite the ongoing droplet coalescence and progressive loss of internal birefringent domains documented by PLM. A transient decrease was observed at Day 8 (−1.0%), reflecting a momentary shift toward solid-like behaviour concurrent with the lamellar ordering event identified by PLM. This transient stiffening was however not sustained: tan δ subsequently returned toward its initial level and continued to drift toward more liquid-like mechanical behavior as the lamellar structure broke down, consistent with the progressive breakdown observed microscopically.

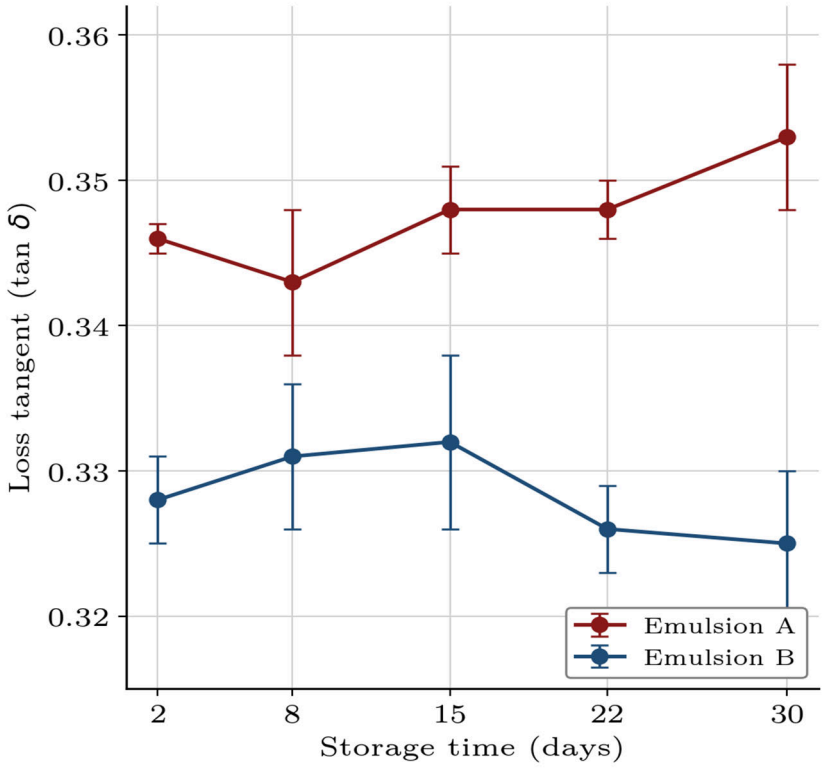

Figure 5. Temporal evolution of the loss tangent (tan δ = G″/G′, frequency-sweep average) during storage at 25 °C for Emulsions A and B. Error bars represent the standard error of the mean (n = 3). Emulsion A displays a near-constant profile (tan δ ≈ 0.346 ± 0.003), with a transient decrease at Day 8 (−1.0%) followed by a gradual drift toward more viscous-like behaviour (+2.0% at Day 30). Emulsion B follows a non-monotonic trajectory: an initial rise to 0.332 at Day 15 (+1.3%) followed by partial recovery to 0.325 at Day 30 (−0.8%), interpreted as thermally induced lamellar reorganization and subsequent network maturation.

Emulsion B displayed a markedly different trajectory. An initial rise in tan δ was observed from Day 2 to Day 15 (+1.3%), followed by a sustained decrease through Day 22–30 (−0.8% relative to Day 2), resulting in a net shift toward more elastic behavior. This non-monotonic pattern mirrors the lamellar consolidation documented by PLM over the same period: an initial reorganization phase followed by genuine mechanical consolidation of the elastic network. The rheological trajectory of Emulsion B thus provides quantitative

mechanical evidence for the progressive maturation of its lamellar architecture, consistently with the sustained birefringence observed under crossed polarizers (Figure 3) and the tan δ data summarized in Table 2.

Table 2. Temporal evolution of the loss tangent (tan δ) for Emulsions A and B at 25 °C. Values are frequency-sweep averages (n = 3), reported as mean ± standard error of the mean. Δ = relative change vs. Day 2.

Day	A (tan δ)	Δ vs. D2	B (tan δ)	Δ vs. D2
2	0.346 ± 0.001	baseline	0.328 ± 0.003	baseline
8	0.343 ± 0.005	−1.0%	0.331 ± 0.005	+1.0%
15	0.348 ± 0.003	+0.5%	0.332 ± 0.006	+1.3%
22	0.348 ± 0.002	+0.5%	0.326 ± 0.003	−0.6%
30	0.353 ± 0.005	+2.0%	0.325 ± 0.005	−0.8%

Statistical note. The small sample size (n = 3 replicates) combined with the inherently narrow range of tan δ values observed here (amplitude of variation < 0.01) precludes robust significance testing: the between-replicate variability is of the same order of magnitude as the effect of interest, leaving any parametric or non-parametric test critically underpowered. The trends described are therefore interpreted on a descriptive basis, supported by the consistency of the pattern across replicates.

Taken together, the rheological data confirm that the structural divergence observed by PLM has measurable macroscopic consequences. The near-constant tan δ profile of Emulsion A is consistent with a network that undergoes progressive structural degradation without a net change in bulk viscoelastic character, masking the underlying breakdown at the frequency-sweep average level. By contrast, the gradual tan δ decline of Emulsion B provides quantitative evidence of network consolidation over storage, a signature directly attributable to the progressive maturation of its lamellar architecture. The temporal resolution and consistency of these trends across three replicates, despite the narrow amplitude of variation, support their mechanistic interpretation.

3.4. Laser Diffraction Analysis

The rheological trajectories were verified at the droplet scale by laser diffraction granulometry, which tracks the coarse fraction independently of network-level reorganization [28]; the Dv50 trajectories are shown in Figure 6. Because the design involves repeated measurements on the same replicate groups across five time points, the data were analysed with a linear mixed-effects model (LMM) rather than pairwise tests, which would violate the independence assumption and could not address whether the two trajectories diverge over time. Emulsion type, storage time (categorical, Day 2 as reference) and their interaction were included as fixed effects, with replicate group as a random intercept: $Dv50 = \beta_0 + \beta_1 \cdot \text{Emulsion} + \beta_2 \text{Time} + \beta_3 \cdot (\text{Emulsion} \times \text{Time}) + u + \varepsilon$, with $u \sim N(0, \sigma^2_u)$ and $\varepsilon \sim N(0, \sigma^2)$.

Emulsion A had an estimated Day 2 Dv50 of 34.66 µm, with Emulsion B systematically lower by 2.18 µm on average (both $p < 0.001$), consistent with the finer droplets conferred by the higher emulsifier concentration. The emulsion × time interaction was non-significant at Day 8 (β = 0.009 µm, $p = 0.991$): both formulations underwent similar early growth, matching the common lamellar structuration event identified at Day 8 by PLM. Beyond Day 8 the trajectories diverged. Emulsion A grew continuously relative to Day 2 (+4.62, +5.41, +6.31 and +6.42 µm at Days 8, 15, 22 and 30; all $p < 0.001$), whereas in Emulsion B the interaction terms were significantly negative at Day 15 (β = −1.83 µm, $p = 0.013$)

and Day 22 (β = −1.93 µm, $p = 0.009$), and negative but no longer significant by Day 30 (β = −1.29 µm, $p = 0.08$).

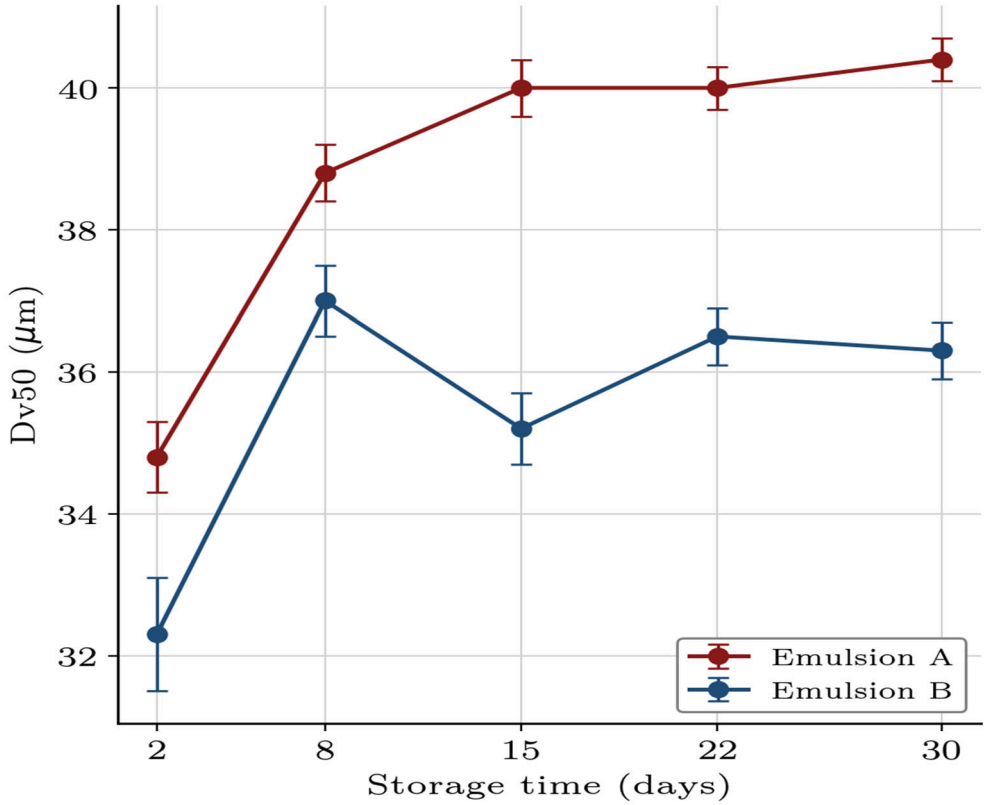

Figure 6. Temporal evolution of the volume median diameter of the coarse fraction (Dv50 > 10 µm) measured by laser diffraction (Mastersizer 3000) at Days 2, 8, 15, 22 and 30 for Emulsions A and B. The shaded band represents the 95% confidence interval (mean ± 1.96 × SEM, $n = 3$). The droplet-level structural changes observed by microscopy were further corroborated by laser diffraction analysis, which quantified the progression of coalescence through changes in coarse-fraction diameter. Emulsion A exhibits continuous and significant particle growth (+6.42 µm at Day 30 vs. Day 2, $p < 0.001$), consistent with active coalescence. Emulsion B shows significantly slower growth, with statistically significant formulation × time interaction terms at Days 15 and 22 ($p < 0.05$), confirming its superior resistance to coalescence. Data analyzed by a linear mixed-effects model (LMM).

Laser diffraction thus grounds the structural narrative in a statistically robust droplet-scale measurement: the progressive Dv50 rise in Emulsion A confirms that lamellar breakdown and mechanical drift translate into physical coalescence, while the stabilization in Emulsion B reflects the protection afforded by a consolidated network. Significant differential growth is resolved from Day 15, more than two weeks before ISO criteria are met, and the low inter-replicate variance (0.105) confirms a genuine formulation effect rather than experimental variability.

4. Discussion

The four techniques converge on a single structural narrative: both formulations cross the same lipid crystallization threshold at Day 8, but only one has sufficient emulsifier concentration to translate this transient ordering event into a mechanically stable, long-lived lamellar gel network.

The shared Day 8 event is the key to interpreting all subsequent observations. On cooling after emulsification, cetearyl alcohol and cetearyl glucoside co-crystallize into interdigitated bilayers that swell with water and assemble into a three-dimensional lamellar

gel network. This process is thermodynamically driven and occurs in both formulations regardless of concentration, which explains why PLM detects a birefringent onset and tan δ shifts transiently toward more solid-like values in both emulsions at Day 8. What the two formulations do not share is the density of inter-bilayer junctions that this crystallization produces: at 2 wt% the bilayer material is insufficient to saturate the available interfacial area and generate a topologically continuous junction network, whereas at 3 wt% the additional emulsifier provides sufficient inter-bilayer junction connectivity to produce a network dense enough to sustain mechanical coherence over time.

In Emulsion A, junction-poor bilayers cannot resist the osmotic and van der Waals pressures that drive inter-lamellar reorganization during storage. As junctions fail, the disjoining pressure maintaining spacing between bilayers drops [29], lamellae collapse locally, and the ordered domains visible under PLM dissolve. The interfacial bilayer coverage around oil droplets degrades in parallel, removing the steric and mechanical barrier to droplet coalescence, which produces the continuous Dv50 increase captured by laser diffraction and the coalescence visible in bright-field microscopy from Day 8 onwards. Tan δ remains near-constant over this period rather than rising, because the progressive loss of elastic network structure is compensated by the increasing viscoelastic contribution of larger, coalescing droplets, a masking effect that makes tan δ a poor indicator of instability in this regime and illustrates why a multi-technique approach is necessary.

In Emulsion B, the junction-rich network formed at 3 wt% generates sufficient disjoining pressure to maintain inter-lamellar spacing and resist reorganization. Rather than dissolving, the lamellar domains mature, as residual disordered bilayer material is progressively incorporated into ordered crystalline domains [17], which is why the birefringent fraction expands monotonically from 66.7% at Day 8 to 98.4% at Day 30. This progressive ordering stiffens the network mechanically, reflected in the sustained tan δ decline from Day 15 to Day 30, while the transient tan δ rise between Day 2 and Day 15 is consistent with a reorganization phase during which bilayer material migrates and junction density redistributes before the network reaches its consolidated architecture. Droplet size remains stable throughout because the dense interfacial coverage provides a continuous barrier against coalescence, confirmed by the non-significant emulsion × time interaction at Day 8 and the significantly negative interaction terms from Day 15 onwards.

The reason ISO testing and Turbiscan turbidimetry fail to detect this divergence is that both measure bulk macroscopic properties that are insensitive to internal bilayer organization. The TSI integrates light backscattering across the entire sample height and is dominated by droplet migration and gross phase separation; it cannot resolve the gradual internal restructuring of lamellar domains within droplets that remain stably dispersed. The three second-tier techniques succeed because each probes a different structural level at which the divergence is physically expressed: PLM the anisotropic optical signature of ordered bilayer domains, oscillatory rheology the mechanical consequence of junction density, and laser diffraction the coalescence that results when interfacial integrity fails. Their convergence from Day 8 to Day 15 is not coincidental, reflecting that junction failure, domain dissolution, interfacial degradation and droplet coalescence are sequential steps in the same underlying process.

The scope of these findings is bounded by the design of the study. A single emulsifier system was examined at two concentrations, in one batch, with three replicates for rheology and laser diffraction and a single measurement for turbidimetry. The convergence of the three second-tier techniques supports the mechanistic interpretation proposed, but its extension to other emulsifier chemistries, other lipid phases and other concentration ranges requires further work.

5. Conclusions

This study demonstrates that a multi-technique analytical protocol integrating oscillatory rheology, laser diffraction granulometry, and AI-assisted polarized light microscopy substantially outperforms both conventional ISO testing and Turbiscan-based industrial screening for the stability assessment of cosmetic emulsions structured by a lamellar gel network. By resolving the structural divergence between a stable and an unstable formulation as early as Day 8 to 15, the protocol achieves a two-to-three week acceleration in time-to-decision relative to the 30-day ISO benchmark, while delivering mechanistic information on lamellar network organization and interfacial film integrity that is entirely inaccessible to macroscopic screening tools.

At the formulation level, the study elucidates the structural mechanism by which a single weight percent increase in Cetearyl Alcohol/Cetearyl Glucoside concentration governs lamellar network fate. At 2 wt%, inter-bilayer junction density is insufficient to resist thermal reorganization: lamellar domains transiently form at Day 8 but progressively dissolve, interfacial film integrity degrades, and droplet coalescence ensues. At 3 wt%, the denser junction network sustains lamellar domains that not only persist but mature, birefringent ordering expands to 98.4% at Day 30, and the network stiffens mechanically as reflected in a sustained loss tangent decline. Two concentrations cannot delimit a threshold, and the transition between network failure and network consolidation is therefore described here as occurring across a 1 wt% increment rather than located at a defined value. This transition is captured convergently by all three second-tier techniques from Day 8 onwards. The result carries direct practical implications for formulation development with Cetearyl Alcohol/Cetearyl Glucoside systems, which are among the most widely used mixed emulsifiers forming lamellar gel networks in sustainable cosmetics owing to their natural origin and compatibility with COSMOS and Ecocert certification frameworks [16].

For industrial formulation development and quality control, these results support integrating loss tangent-based oscillatory rheology, AI-assisted polarized light microscopy, and laser diffraction granulometry as a coupled second-tier protocol alongside or in place of Turbiscan-based single-technique screening. The practical gain is threefold: a two to three week reduction in time-to-decision, structural and mechanistic insight that directly guides reformulation decisions when instability is detected, and quantitative discrimination between formulations that appear macroscopically equivalent but follow structurally divergent trajectories.

Author Contributions: Conceptualization, A.V., R.C. and B.A.; methodology, A.V. and P.P.; software, A.V.; formal analysis, A.V., M.C.-B. and C.S.; investigation, A.V. and P.P.; resources, B.A.; data curation, A.V.; writing—original draft, A.V.; writing—review and editing, A.V., R.C., M.C.-B. and C.S.; visualization, A.V. All authors have read and agreed to the published version of the manuscript.

Funding: This research was funded by SICAF Cosmétiques, as part of a collaboration with the Faculty of Pharmacy and the Faculty of Sciences of Aix-Marseille University.

Institutional Review Board Statement: Not applicable.

Informed Consent Statement: Not applicable.

Data Availability Statement: Data will be made available on request.

Acknowledgments: The project is the result of a collaboration between the Faculty of Pharmacy of Aix-Marseille University, the Faculty of Sciences of Aix-Marseille University, and the company SICAF, which funded the project. During the preparation of this work, the author(s) used Claude Sonnet 5 (Anthropic) for language editing and readability improvements, manuscript structuring, and verification and formatting of bibliographic references. The author(s) reviewed and edited the output as needed and take full responsibility for the content of the published article.

Conflicts of Interest: The authors declare that this research was funded by SICAF, with which two of the authors (Axel Viton and Béatrice Anthouard) are affiliated. The authors declare no other competing financial interests or personal relationships that could have influenced the work reported in this paper.

References

1. *ISO/TR 18811:2018*; International Organization for Standardization. Cosmetics—Guidelines for the Stability Testing of Cosmetic Products. ISO: Geneva, Switzerland, 2018.
2. Viton, A.; Coatmeur, R.; Anthouard, B.; Claeys-Bruno, M.; Piccerelle, P. Anticipating cosmetic emulsion stability using a novel multi-analytical approach. *Int. J. Cosmet. Sci.* **2025**, *48*, 589–599. [CrossRef] [PubMed]
3. Tadros, T.F. *Emulsion Formation and Stability*; Wiley-VCH: Weinheim, Germany, 2013.
4. Junginger, H.E. Colloidal structures of O/W creams. *Pharm. Weekbl. Sci.* **1984**, *6*, 141–149. [CrossRef] [PubMed]
5. Eccleston, G.M. Functions of mixed emulsifiers and emulsifying waxes in dermatological lotions and creams. *Colloids Surf. A Physicochem. Eng. Asp.* **1997**, *123–124*, 169–182. [CrossRef]
6. Colafemmina, G.; Palazzo, G.; Mateos, H.; Amin, S.; Fameau, A.L.; Olsson, U.; Gentile, L. The cooling process effect on the bilayer phase state of the CTAC/cetearyl alcohol/water surfactant gel. *Colloids Surf. A* **2020**, *597*, 124821. [CrossRef]
7. Datta, A.; Tanmay, V.S.; Tan, G.X.; Reynolds, G.W.; Jamadagni, S.N.; Larson, R.G. Characterizing the rheology, slip, and velocity profiles of lamellar gel networks. *J. Rheol.* **2020**, *64*, 851–862. [CrossRef]
8. Cunningham, G.E.; Alberini, F.; Simmons, M.J.H.; O'Sullivan, J.J. Understanding the effects of processing conditions on the formation of lamellar gel networks using a rheological approach. *Chem. Eng. Sci.* **2021**, *242*, 116752. [CrossRef]
9. Ribeiro, H.M.; Morais, J.A.; Eccleston, G.M. Structure and rheology of semisolid o/w creams containing cetyl alcohol/non-ionic surfactant mixed emulsifier and different polymers. *Int. J. Cosmet. Sci.* **2004**, *26*, 47–59. [CrossRef] [PubMed]
10. Tsurusawa, H.; Leocmach, M.; Russo, J.; Tanaka, H. Direct link between mechanical stability in gels and percolation of isostatic particles. *Sci. Adv.* **2019**, *5*, eaav6090. [CrossRef] [PubMed]
11. Hill, K.; von Rybinski, W.; Stoll, G. *Alkyl Polyglycosides: Technology, Properties, and Applications*; Wiley-VCH: Weinheim, Germany, 2008.
12. Eccleston, G.M. Emulsions and creams. In *Aulton's Pharmaceutics: The Design and Manufacture of Medicines*, 5th ed.; Aulton, M.E., Taylor, K.M.G., Eds.; Elsevier: Edinburgh, UK, 2018; pp. 446–475.
13. Tadros, T.F. *Applied Surfactants: Principles and Applications*; Wiley-VCH: Weinheim, Germany, 2005.
14. Terescenco, D.; Savary, G.; Clemenceau, F.; Merat, E.; Duchemin, B.; Grisel, M.; Picard, C. The alkyl polyglucoside/fatty alcohol ratio effect on the formation of liquid crystal phases in binary systems. *J. Mol. Liq.* **2018**, *253*, 45–52. [CrossRef]
15. Ahmadi, D.; Mahmoudi, N.; Heenan, R.K.; Barlow, D.J.; Lawrence, M.J. The influence of co-surfactants on lamellar liquid crystal structures formed in creams. *Pharmaceutics* **2020**, *12*, 864. [CrossRef] [PubMed]
16. *COSMOS Standard v3.0*; COSMOS-Standard AISBL. COSMOS-Standard: Brussels, Belgium, 2021. Available online: https://www.cosmos-standard.org (accessed on 20 March 2026).
17. de Vringer, T.; Joosten, J.G.H.; Junginger, H.E. A study of the ageing of the gel structure in a nonionic O/W cream by X-ray diffraction, differential scanning calorimetry and spin-lattice relaxation measurements. *Colloid Polym. Sci.* **1987**, *265*, 448–457. [CrossRef]
18. Teeranachaideekul, V.; Soontaranon, S.; Sukhasem, S.; Chantasart, D.; Wongrakpanich, A. Influence of the emulsifier on nanostructure and clinical application of liquid crystalline emulsions. *Sci. Rep.* **2023**, *13*, 4185. [CrossRef] [PubMed]
19. Mengual, O.; Meunier, G.; Cayré, I.; Puech, K.; Snabre, P. TURBISCAN MA 2000: Multiple light scattering measurement for concentrated emulsion and suspension instability analysis. *Talanta* **1999**, *50*, 445–456. [CrossRef] [PubMed]
20. Oquab, M.; Darcet, T.; Moutakanni, T.; Vo, H.V.; Szafraniec, M.; Khalidov, V.; Fernandez, P.; Haziza, D.; Massa, F.; El-Nouby, A.; et al. DINOv2: Learning robust visual features without supervision. *arXiv* **2023**, arXiv:2304.07193.
21. Dosovitskiy, A.; Beyer, L.; Kolesnikov, A.; Weissenborn, D.; Zhai, X.; Unterthiner, T.; Dehghani, M.; Minderer, M.; Heigold, G.; Gelly, S.; et al. An image is worth 16×16 words: Transformers for image recognition at scale. *arXiv* **2021**, arXiv:2010.11929.
22. Caron, M.; Touvron, H.; Misra, I.; Jégou, H.; Mairal, J.; Bojanowski, P. Emerging properties in self-supervised vision transformers. *arXiv* **2021**, arXiv:2104.14294.
23. MacQueen, J. Some methods for classification and analysis of multivariate observations. In Proceedings of the 5th Berkeley Symposium on Mathematical Statistics and Probability, Berkeley, CA, USA, 21 June–18 July 1965; Volume 1, pp. 281–297.
24. Savitzky, A.; Golay, M.J.E. Smoothing and differentiation of data by simplified least squares procedures. *Anal. Chem.* **1964**, *36*, 1627–1639. [CrossRef]
25. McClements, D.J. Critical review of techniques and methodologies for characterization of emulsion stability. *Crit. Rev. Food Sci. Nutr.* **2007**, *47*, 611–649. [CrossRef] [PubMed]

26. Seabold, S.; Perktold, J. Statsmodels: Econometric and statistical modeling with Python. In Proceedings of the 9th Python in Science Conference (SciPy 2010), Austin, TX, USA, 28 June–3 July 2010; pp. 92–96.
27. Mezger, T.G. *The Rheology Handbook*, 4th ed.; Vincentz Network: Hanover, Germany, 2020.
28. Santos, J.; Calero, N.; Trujillo-Cayado, L.A.; Garcia, M.C.; Muñoz, J. Assessing differences between Ostwald ripening and coalescence by rheology, laser diffraction and multiple light scattering. *Colloids Surf. B Biointerfaces* **2017**, *159*, 405–411. [CrossRef] [PubMed]
29. Bergeron, V. Forces and structure in thin liquid soap films. *J. Phys. Condens. Matter* **1999**, *11*, R215–R238. [CrossRef]

Disclaimer/Publisher's Note: The statements, opinions and data contained in all publications are solely those of the individual author(s) and contributor(s) and not of MDPI and/or the editor(s). MDPI and/or the editor(s) disclaim responsibility for any injury to people or property resulting from any ideas, methods, instructions or products referred to in the content.